Nano Research
2019, 12(7): 1619–1624

ISSN 1998-0124 CN 11-5974/O4
https://doi.org/10.1007/s12274-019-2401-0

Research Article

Analysis of photoluminescence behavior of high-quality single-layer MoS_2

Lu Xu, Liyun Zhao, Yunsong Wang, Mingchu Zou, Qing Zhang, and Anyuan Cao (✉)

Department of Materials Science and Engineering, College of Engineering, Peking University, Beijing 100871, China

Received: 28 November 2018 / **Revised:** 3 March 2019/ **Accepted:** 14 March 2019

ABSTRACT

The ability to tailor and enhance photoluminescence (PL) behavior in two-dimensional (2D) transition metal dichalcogenides (TMDCs) such as molybdenum disulfide (MoS_2) is significant for pursuing optoelectronic applications. To achieve this, it has been essential to obtain high-quality single-layer MoS_2 and fully explore its intrinsic PL performance. Here, we fabricate single-layer MoS_2 by a thermal vapor sulfurization method in which a pre-deposited molybdenum trioxide (MoO_3) thin film is sulfurized over a short period (for several minutes) to turn into MoS_2. These as-grown MoS_2 crystals show quite strong PL, which is about one order of magnitude higher than that of chemical-vapor-deposited MoS_2. Temperature- and power-dependent spectroscopy measurements disclose the apparent influence of sulfur (S) vacancies on the PL behavior and the noticeable free-to-bound exciton recombinations in the luminescence process. The fact that PL intensity of the sample in vacuum sharply lowered down relative to in air reveals that the high PL is facilitated by molecular adsorption on S vacancies in air. And multi-channel decay processes coupled with S vacancies are revealed in the time-resolved PL spectroscopy. In our work, single-layer MoS_2 with high PL is synthesized and its defect-induced PL features are analyzed, which is of great importance for developing advanced nano-electronics and optoelectronics based on 2D structures.

KEYWORDS

MoS_2, photoluminescence, thermal vapor sulfurization, S vacancy

1 Introduction

Two-dimensional (2D) transitional metal dichalcogenides (TMDCs) provide an ideal platform for fundamental understanding of low-dimensional phenomena and related physics, as well as for constructing functional optoelectronic devices such as those based on van der Waals heterojunctions [1–3]. Molybdenum disulfide (MoS_2) is a typical TMDC, and unlike the zero-bandgap graphene, it is a semiconductor, with an indirect-to-direct bandgap transformation when the material is thinned to a single layer [4]. Consequently, the photoluminescence (PL) from monolayer MoS_2 promises many exciting applications in nanoelectronics and optoelectronics such as photovoltaics, light emitters, photoelectrochemistry and photodetectors [5, 6]. Hence, we have seen extensive studies on controlled fabrication of MoS_2 films and continuous efforts toward optimized PL performance [7, 8]. For example, enhanced PL was demonstrated in MoS_2 layers suspended from substrate or separated by polyelectrolyte molecules in a layer-by-layer assembly [9]. Microscale metal spiral rings were deposited on MoS_2 to induce exciton-plasma interaction with spin-orbit coupling of light and therefore enhance PL [10]. Also, it was reported that the quantum yield of chemical-vapor-deposited MoS_2 can be improved greatly after treatment with organic superacid [11]. Recently, depositing graphene quantum dots onto the MoS_2 surface resulted in a n-doping effect that could modify the PL performance [12]. Despite all these efforts, there is still a lot of room to improve the PL properties of as-obtained MoS_2 so that the optimized PL is highly stable and no foreign materials are needed.

Except for the anticipated PL performance, another compelling feature of MoS_2 is that this 2D material is active and adsorptive with abundant active sites like edges and defects. And as such, extensive studies have been done on MoS_2 focusing on its applications in fields such as photocatalysis and gas sensing [13, 14]. Among its multiple kinds of defects, S vacancies are the most common ones in MoS_2 whether exfoliated from natural bulk or synthesized by bottom-up strategies. Chemical synthesis methods are universally used to obtain homogeneous high-quality single-layer MoS_2, and it is inevitable to have built-in S vacancies in MoS_2 crystals formed under high-temperature conditions. So, to understand the impacts of the intrinsic defects on its PL behaviors has become important for further studies on PL related applications. According to previous studies, S vacancies, as potential non-radiative recombination centers, were assumed to undermine the PL performance [15]. However, studies also revealed enhancing effects from S vacancies in air environment [16]. Therefore, controlled synthesis of MoS_2 and a careful study on PL properties are needed to give an insight into the influence of S vacancies.

Here, we take a thermal vapor sulfurization (TVS) method, in which MoO_3 thin film is evenly pre-deposited and then uniformly sulfurized over the substrates. It is, in some ways, more controllable and reliable, compared with chemical vapor deposition (CVD) method consisting of a gaseous precursor from upstream MoO_3 powder. We show that monolayer MoS_2 synthesized by TVS (TVS-MoS_2) could produce uniform and strong PL emission without the need of chemical functionalization or further treatment, with an intensity exceeding 10 times that of monolayer MoS_2 by CVD (CVD-MoS_2). We further do in-depth experiments to analyze PL properties of our TVS-MoS_2 and reveal its S-vacancy-featured

Address correspondence to anyuan@pku.edu.cn

behaviors. In temperature-dependent spectroscopy measurements, a low-temperature-only peak arises, disclosing the apparent influence of S vacancies on the PL behaviors. And the fact that PL intensity of the sample in vacuum drops sharply relative to in air reveals that the high PL is facilitated by molecular adsorption on S vacancies in air. The S-vacancy-induced feature is also indicated by the sub-linear power dependency coefficient which reflects the evident free-to-bound exciton recombinations in PL process. In addition, multi-channel decay processes coupled with S vacancies are embodied in the time-resolved PL spectroscopy. Our results demonstrate that TVS is a reliable method to synthesize monolayer MoS_2 with excellent optical properties, and the influences of S vacancies on PL behaviors are fully reflected. This can be meaningful for MoS_2 fabrication and its optical applications.

2 Experimental

2.1 Preparation of substrates

The sapphire substrates with *c* orientation (0001 plane) all have standard size of 10 mm × 10 mm × 0.43 mm. Firstly, piranha solution is prepared for use of hydrophilization treatment. It consists of H_2SO_4 and 30% H_2O_2 in a volume ratio of 7:3. Substrates are immersed in piranha solution for 30 min, kept at 80 °C, and then rinsed in deionized water three times to eliminate piranha solution. In this way, the substrates become hydrophilic, which is beneficial to precursor absorption and MoS_2 crystallization. Subsequently, MoO_3 is thermally evaporated onto sapphire substrates in a vacuum chamber. In the evaporation process, the pressure is kept at 1.0×10^{-4} Pa and evaporation rate is 0.2 Å/s, monitored by a thickness meter. As a result, substrates are covered with MoO_3 film of designed thickness.

2.2 TVS synthesis of MoS_2

MoS_2 is synthesized by thermal vapor sulfurization in atmospheric pressure. Sapphire substrates are put in a 1-inch quartz tube, placed at downstream of gas flow. Sulfur powder is placed at upstream out of the furnace heating zone (Fig. 1(a)). Argon is used as carrier gas and is sent through the tube 30 minutes before temperature ramping up to remove air and water. Substrate zone is heated by the furnace with a temperature rising rate of 25 °C/min. Sulfur powder outside the furnace is heated by a heating belt. Sulfur reaches the setting temperature of 103 °C right at the time when substrate zone reaches 700 °C. Substrates are kept at 750 °C for several minutes and after this immediately experience nature cooling.

2.3 SEM, AFM, XPS, Raman/PL, TRPL measurements

The TVS-grown MoS_2 was first characterized in scanning electron microscopy (SEM, Hitachi S-4800). And atomic force microscopy (AFM, Bruker, Nanoscope V, Multimode 8) is used to display surface information. Raman/PL measurements were conducted using a Raman spectroscopy (Horiba, iHR-550) with a 532 nm laser. Laser power was adjusted using neutral density filters (20 μW–1 mW), and the lasers were focused onto sample with a 100× objective lens (number aperture, NA = 0.9). Valence states and element ratio of S and Mo were inspected by X-ray photoelectron spectroscopy (XPS, Kratos Analytical Ltd. Axis Ultra). Time-resolved PL (TRPL) was measured using a lifetime spectrometer (Edinburgh, FLS980).

3 Results and discussion

Bottom-up methods for synthesizing MoS_2 usually use either MoO_3 powders (in CVD) or a thin solid MoO_3 film (in TVS) as Mo-source for sulfurizing [17]. Here, we adopt the TVS method since a pre-deposited MoO_3 film allows rapid and uniform sulfurizing over the substrate to grow MoS_2. We also delay the vaporizing of sulfur powder at the upstream until the reaction zone where MoO_3-coated substrates are placed is heated to nearly the reaction temperature, and terminate the growth process after a short period of several minutes (illustrated in Fig. 1(a), see Experimental methods for details). An appropriate thickness of ~ 0.6 nm is determined by comparing samples synthesized from MoO_3 film thicknesses from 0.6 to 2.6 nm (Fig. S1 in the Electronic Supplementary Material (ESM)). Also, other growth parameters like substrates, timing of S supply and gas flow that can make a difference to the resultant MoS_2 crystals are optimized and discussed in Figs. S2–S4 in the ESM. In a typical sample characterized by SEM, triangular MoS_2 flakes have grown into lateral sizes up to about 30 μm, exhibiting a smooth and clean surface (Fig. 1(b)). The surface topography and height information of MoS_2 flakes are measured by AFM through a

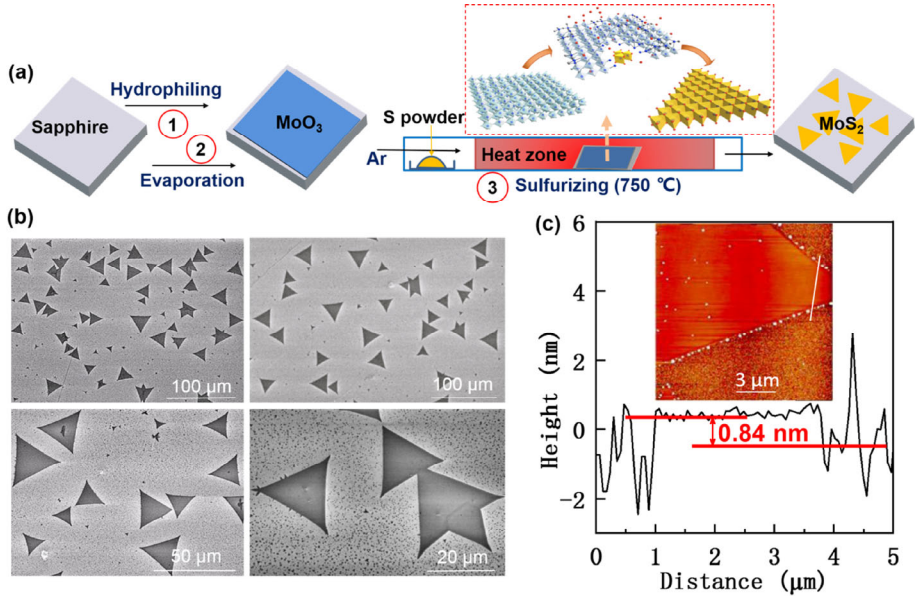

Figure 1 Synthesis and characterization of TVS-MoS_2. (a) Schematic illustration of the preparation process of single-layer MoS_2 crystals, following three procedures of hydrophiling treatment, evaporation of MoO_3 and sulfurizing MoO_3 in high-temperature furnace. (b) SEM images at different magnifications from typical samples, showing the uniformly distributed up-to-30-μm triangle sheets with clean surfaces. (c) Height information from AFM measurement along the white line in the inset. The inset is an overall AFM profile of this region.

15 μm × 15 μm region (Inset of Fig. 1(c)). Linear scanning profile shows a constant height of ~ 0.84 nm across the flake area, consistent with a single-layer sheet anchored on substrate (Fig. 1(c)).

Raman spectroscopy is an effective way to examine crystalline quality, and layer numbers specifically for 2D MoS_2 materials [18]. Representative Raman signal from as-synthesized individual MoS_2 triangular sheet is displayed in Fig. 2(a). Respectively, peaks E^1_{2g} (385.4 cm^{-1}) and A_{1g} (404.7 cm^{-1}) are resulted from the in-plane and out-of-plane vibration modes of displacement of S atoms relative to Mo atoms (as the inset of Fig. 2(a) shows), and a difference of 19.3 cm^{-1} is in well accordance with the single-layer characteristic in precious reports [19]. As for intensities, the peaks of TVS-MoS_2 are slightly higher than that of CVD-MoS_2 measured under the same conditions, indicating comparable crystalline quality. PL spectrum of the TVS-MoS_2 shows only one single prominent peak centered at ~ 1.865 eV in ambient conditions (Fig. 2(b)). In particular, the averaged PL intensity of different TVS-MoS_2 flakes exceeds 10 times that of CVD-MoS_2 measured under the same condition (1 mW laser power, 1 s integral time), as can be seen in Fig. 2(b) and the inset. Raman mapping is homogeneous throughout the crystal surface (Fig. 2(d)), and PL mapping from the same flake is relatively uniform on the whole (Fig. 2(e)), indicating that this TVS method yields high-quality single-layer MoS_2 with uniform optical properties. Here in the PL mapping, it is slightly weakened at some inner sites and along the edge. As for the inner sites, the PL intensity is weakened probably because of flaws in the crystal or particles on the surface that might be induced during high-temperature growth process or impurities in lab air. When it comes to the edges, since the laser spot with a diameter is not entirely on the crystal, the PL intensity becomes weaker.

We then studied low-temperature PL behaviors. Figure 3(a) shows a sequence of PL spectra at temperatures ranging from 290 K down to the lowest attainable temperature 77 K. It is notable that when the temperature is lowered down to 150 K and below, a new wide peak appears at lower energy and its position shifts from 1.7 eV at 150 K to 1.8 eV at 77 K. According to previous reports, this low-temperature-only peak is attributed to defect-bounded excitons associated with S vacancies [20]. Since the binding energy of free excitons bound to defects is low, bound excitons are easy to dissociate when temperature is lifted, so the peak gradually diminishes with increasing temperature and disappears above 150 K. The mechanism of broadening of this peak might be a comprehensive thermodynamics and kinetics process, involving in band transitions with changes of charged states, as analyzed in previous literature [21]. As for the main peak, it becomes more intense and narrow with a blue-shift trend when temperature decreases, because of a widened bandgap from lattice shrinkage and less thermal relaxations at low temperature. The values of peak positions for each temperature are read out and listed in Fig. 3(b). Varshni equation $E_g(T) = E_g(0) - \alpha T^2 / (T + \beta)$ is used to quantify the relationship between temperature (T) and band gap (E_g) of many semiconductors, in which α is the bandgap energy temperature coefficient and β is a constant close to the Debye temperature of the material [22]. We obtain fitting results as follows: $E_g(0)$ =1.945 ± 0.03 eV, α = (3.76 ± 0.47) × 10^{-4} eV/K, β = 124 ± 64 K for peak H. $E_g(0)$ is comparable to the fitted result of 1.874 eV in a previous literature [23]. In addition, the intensities of PL peak increase monotonic with decreasing temperature on the whole (Fig. 3(c)). At a temperature as low as 77 K, exciton decay processes are dominated by radiative recombinations that account for high PL intensity. This is because non-radiative recombinations requiring participation of phonons are inhibited at low temperature, giving way to radiative recombinations. And at room temperature, PL intensity is lowered as a result of more severe non-radiative recombinations.

Previous studies have demonstrated that the PL intensity of MoS_2 would change under different air pressures as a result of molecule adsorption at S vacancies [24]. To reveal the influence of air, we conducted *in-situ* PL measurements both in air and vacuum at room temperature. In vacuum, the PL intensity receded to about one fourth of the value in air, and bounced back to approximately

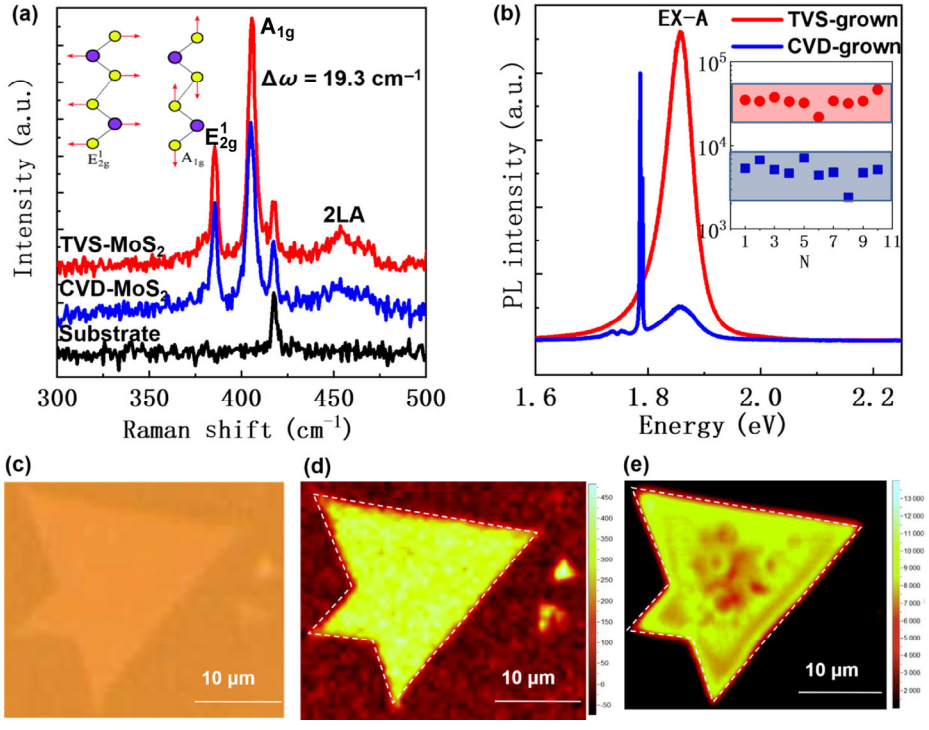

Figure 2 Raman/PL spectra and/or mappings of TVS-MoS_2 and CVD-MoS_2. (a) Raman signals of TVS-MoS_2 and CVD-MoS_2. (b) PL properties of TVS-MoS_2 and CVD-MoS_2. The sharp peak at about 1.8 eV is from the substrate (sapphire). Inset is the PL intensities of randomly picked ten points form both TVS-MoS_2 and CVD-MoS_2. (c) Optical microscopy image of a MoS_2 sheet showing (d) uniform Raman mapping, and (e) strong and relatively uniform PL mapping throughout the crystal surface.

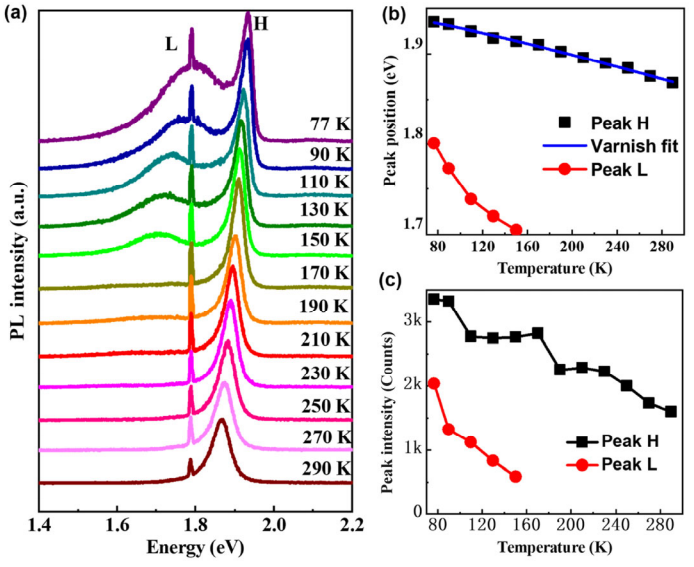

Figure 3 Temperature-correlated PL properties of TVS-MoS_2. (a) PL spectra under a series of temperatures ranging from 290 to 77 K. A defect-induced peak appears at 150 K and below. Both peaks become more intense, more narrow with a blue-shift when temperature becomes lower. (b) The peak energies and (c) the peak intensities versus temperature are read out from (a). The energy of peak H well fits the Varnish equation with $E_g(0) = 1.945$ eV.

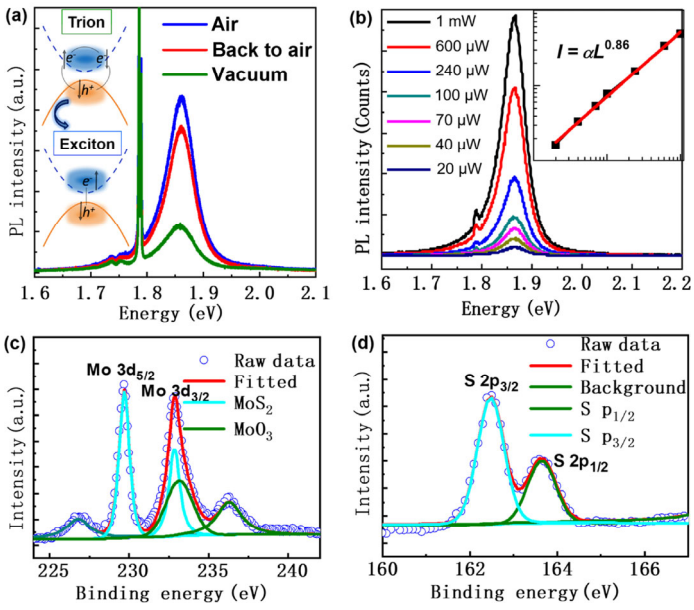

Figure 4 PL behaviors under different conditions and XPS measurements of TVS-MoS_2. (a) PL spectra of TVS-MoS_2 in different air conditions. In vacuum, the intensity decreases to only one fourth of that in air, and can recover approximately to the previous level when back in air. (b) PL spectra of TVS-MoS_2 under laser powers from 1 mW to 20 μW. Correspondingly, linear fit of logarithmic PL intensities versus logarithmic laser powers are presented in the inset. (c) and (d) are XPS of as-grown MoS_2 displaying peaks for Mo 3d and S 2p, respectively. We tentatively get a rough estimation of the ratio of S and Mo atoms as 1.635 by using quantitative peak areas.

the original value upon exposure to air again (Fig. 4(a)). This enhancement associated with air is due to interaction between air molecules and S vacancies in MoS_2. In vacuum, excessive electrons caused by n-doping effect from S vacancies would join hole-electron pairs to form trions, and may also screen the radiative transitions of excited hole-electron pairs. Once it is exposed to air, acceptor-like molecules such as oxygen and nitrogen will adsorb onto the vacancy sites and act as charge transfer channels to deplete excessive electrons and consequently revert trions to excitons [24]. The schematic diagram of trion radiative recombination turning into exciton radiative recombination is depicted in the inset of Fig. 4(a). Thus in air, the intensity of luminescence from excited hole-electron pairs can be well displayed owing to molecular adsorption on S vacancies. The change in PL intensity under air or vacuum conditions is reversible.

To further disclose the recombination types of excitons associated with S vacancies, we analyzed excitation power-dependent PL spectra. An exponential equation $I = \alpha L^n$ can be used to describe the relationship between PL intensity (I) and laser power (L), where α is the coefficient and the exponent n corresponds to recombination type of excitons. Specifically, $n = 1$ for pure free-exciton recombination and $n = 0.5$ for bound-exciton recombination. If n falls between 0.5 and 1, the PL peak should be attributed to free-to-bound recombinations [25]. We obtained PL spectra of TVS-MoS_2 (Fig. 4(b)) under different laser power ranging from 20 μW to 1 mW. Heating effect can be neglected. A well fitted result of $n = 0.86$ indicates that excitons are not completely free and take the free-to-bound recombination mode (inset of Fig. 4(b)). Generally, free-to-bound recombinations include a free electron recombining with a neutral acceptor, or a free hole recombining with a neutral donor [25]. In our sample, this is supposed to take place between free holes and bound electrons at S vacancy sites. Usually, if limited by the contents of S vacancy sites, the PL intensity produced from free-to-bound recombinations would rise relatively slowly till saturation. However, this saturation trait is not apparent in TVS-MoS_2 probably because of the abundance of S vacancy sites in our case.

XPS, which can provide valence states of elements on surface and quantitative information for layers at atomic scale (since the thickness of single layer MoS_2 is about 0.8 nm, which can be covered by the probing depth of XPS), is adopted to tentatively quantify S vacancies. In Mo 3d spectra (Fig. 4(c)), Mo^{4+} doublet is dissolved, with $3d_{5/2}$ peak at 229.70 eV and $3d_{3/2}$ peak at 232.85 eV, and the difference of 3.15 eV well coincides with the spin-orbit splitting energy of Mo^{4+}. Also, there is Mo^{6+} doublet coming from the residual MoO_3 due to short sulfurizing duration in TVS process. In S 2p spectra (Fig. 4(d)), S^{2-} doublet is dissolved into $2p_{3/2}$ peak at 162.48 eV and $2p_{1/2}$ peak at 163.68 eV, with a 1.16 eV difference corresponding to the spin-orbit splitting energy of S^{2-}. The values of integrated areas under Mo^{4+} and S^{2-} doublets over their sensitivity factors (3.321 and 0.668 for Mo and S, respectively) denote the contents of bonded elements. Thus we obtain atomic concentrations of Mo^{4+} and S^{2-} to be 37.9% and 62.1%, corresponding to a S:Mo atom ratio of 1.635, which is much lower than those measured either in mechanically exfoliated MoS_2 or CVD synthesized MoS_2 (typically around or above 1.8) [26, 27]. This verifies the existence of a significant amount of S vacancies within the MoS_2 crystal, which is a stable and equilibrium structure formed at high temperature, as a result of fast and uniform sulfurizing of pre-deposited MoO_3 film.

TRPL measurements are conducted to understand exciton decay processes and underlying dynamics. The decay dynamics of room-temperature TRPL (Fig. 5) can be best fitted by a tri-exponential decay function, with three characteristic lifetimes including $\tau_1 =$ 85.7 ps, $\tau_2 = 930$ ps and $\tau_3 = 4.63$ ns (Table 1). Exciton dynamics usually involve complex processes with different recombination channels such as exciton-exciton annihilation, phonon scattering, electron-hole recombination and surface trapping. There have been many discussions over the lifetime scale of each channels [28–30]. According to previous studies, the short lifetime of 85.7 ps is most likely to fall to the defect-assisted Auger processes [23]. For the middle lifetime of 930 ps, we tentatively assign it to the interband electron-hole radiative recombination, referring to a magnitude of several hundred ps proposed by either calculated values or measured results [28, 31]. The rather slow decay at 4.63 ns is attributed to surface trapping by defects, which is believed to account for the long lifetime as well as high PL intensity [32]. When it comes to 77 K,

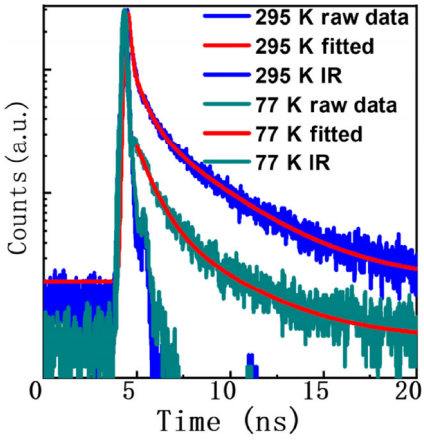

Figure 5 Time-resolved PL from MoS_2 recorded at 295 and 77 K, respectively. The red lines are fitting curves with a three-exponential decay function for 295 K and a bi-exponential decay function for 77 K.

Table 1 Lifetimes of exciton decay dynamics at 295 and 77 K from TRPL measurements

Temperature	τ_1 (defect-assisted Auger process)	τ_2 (interband electron-hole combinations)	τ_3 (surface trapping)
295 K	85.7 ps	930 ps	4.63 ns
77 K	—	863 ps	3.55 ns

only two recombination channels can be observed. The TRPL curve is best fitted by a bi-exponential decay function, with two characteristic lifetimes of 863 ps and 3.548 ns. The fast process in tens of ps that can be observed at room temperature is vanished at 77 K, possibly owing to the decreasing of multiexciton interaction and then Auger recombiniation. Lifetimes of TRPL at 295 and 77 K are listed in Table 1.

4 Conclusion

In conclusion, TVS is a reliable method to uniformly and fast synthesize MoS_2 single-layer crystals. The PL of as-grown MoS_2 is prominent and sharp with the intensity an order of magnitude higher than that of CVD-MoS_2. Such enhancing effect is verified to come from S vacancies assisted by air molecules. The influence of abundant S vacancies is confirmed by low-temperature PL spectra and revealed in power-dependent measurements, further disclosed by the complex decay dynamics in TRPL as well. This facile and controllable method might be applied to obtain other TMDCs with high optical quality, which would facilitate applications in areas such as light emitters and photo-detectors based on TMDCs.

Electronic Supplementary Material: supplementary material (SEM characterization and comparison of MoS_2 samples grown under different TVS conditions and parameters such as the MoO_3 thickness, substrate type, sulfur supplying time and gas flow) is available in the online version of this article at https://doi.org/10.1007/s12274-019-2401-0.

Acknowledgements

This work was supported by the National Natural Science Foundation of China (No. 51672005) and the National Key R&D Program of China (No. 2016YFE0127300).

References

[1] Xia, M.; Li, B.; Yin, K. B.; Capellini, G.; Niu, G.; Gong, Y. J.; Zhou, W.; Ajayan, P. M.; Xie, Y. H. Spectroscopic signatures of AA' and AB stacking of chemical vapor deposited bilayer MoS_2. *ACS Nano* **2015**, *9*, 12246–12254.

[2] Kim, I. S.; Sangwan, V. K.; Jariwala, D.; Wood, J. D.; Park, S.; Chen, K. S.; Shi, F. Y.; Ruiz-Zepeda, F.; Ponce, A.; Jose-Yacaman, M. et al. Influence of stoichiometry on the optical and electrical properties of chemical vapor deposition derived MoS_2. *ACS Nano* **2014**, *8*, 10551–10558.

[3] Ceballos, F.; Bellus, M.Z.; Chiu, H. Y.; Zhao, H. Ultrafast charge separation and indirect exciton formation in a MoS_2–$MoSe_2$ van der waals heterostructure. *ACS Nano* **2014**, *8*, 12717–12724.

[4] Mak, K. F.; Lee, C.; Hone, J.; Shan, J.; Heinz, T. Atomically thin MoS_2: A new direct-gap semiconductor. *Phy. Rev. Lett.* **2010**, *105*, 136805.

[5] Cheng, R.; Li, D. H.; Zhou, H. L.; Wang, C.; Yin, A. X.; Jiang, S.; Liu, Y.; Chen, Y.; Huang, Y.; Duan, X. Electroluminescence and photocurrent generation from atomically sharp WSe_2/MoS_2 heterojunction *p*–*n* diodes. *Nano Lett.* **2014**, *14*, 5590−5597.

[6] Galfsky, T.; Sun, Z.; Considine, C. R.; Chou, C. T.; Ko, W. C.; Narimanov, E. E.; Menon, V. M. Broadband enhancement of spontaneous emission in two-dimensional semiconductors using photonic hypercrystals. *Nano Lett.* **2016**, *16*, 4940−4945.

[7] Wan, Y.; Zhang, H.; Wang, W.; Sheng, B. W.; Zhang, K.; Wang, Y. L.; Song, Q. J.; Mao, N. N.; Li, Y. P.; Wang, X. et al. Origin of improved optical quality of monolayer molybdenum disulfide grown on hexagonal boron nitride substrate. *Small* **2016**, *12*, 198–203.

[8] Joo, P.; Jo, K.; Ahn, G.; Voiry, D.; Jeong, H. Y.; Ryu, S.; Chhowalla, M.; Kim, B. S. Functional polyelectrolyte nanospaced MoS_2 multilayers for enhanced photoluminescence. *Nano Lett.* **2014**, *14*, 6456−6462.

[9] Yu, Y. F.; Yu, Y. L.; Xu, C.; Cai, Y. Q.; Su, L. Q.; Zhang, Y.; Zhang, Y. W.; Gundogdu, K.; Cao, L. Y. Engineering substrate interactions for high luminescence efficiency of transition-metal dichalcogenide monolayers. *Adv. Funct. Mater.* **2016**, *26*, 4733–4739.

[10] Li, Z. W.; Li, Y.; Han, T. Y.; Wang, X. L.; Yu, Y.; Tay, B.; Liu, Z.; Fang, Z. Y. Tailoring MoS_2 exciton−plasmon interaction by optical spin−orbit coupling. *ACS Nano* **2017**, *11*, 1165–1171.

[11] Amani, M.; Burke, R. A.; Ji, X.; Zhao, P. D.; Lien, D. H.; Taheri, P.; Ahn, G. H.; Kirya, D.; Ager, III J. W.; Yablonovitch, E. et al. High luminescence efficiency in MoS_2 grown by chemical vapor deposition. *ACS Nano* **2016**, *10*, 6535−6541.

[12] Li, Z. W.; Ye, R. Q.; Ye, R.; Kang, Y. M.; Zhu, X.; Tour, J. M.; Fang, Z. Y. Graphene quantum dots doping of MoS_2 monolayers. *Adv. Mater.* **2015**, *27*, 5235–5240.

[13] Kwon, K. C.; Choi, S.; Hong, K.; Moon, C. W.; Jang, D. H.; Kim, T.; Sohn, W.; Jeon, J. M.; Lee, J. M.; Nam, K. T. et al. Wafer-scale transferable molybdenum disulfide thin-film catalysts for photoelectrochemical hydrogen production. *Energy Environ. Sci.* **2016**, *9*, 2240–2248.

[14] Perkins, F. K.; Friedman, A. L.; Cobas, E.; Campbell, P. M.; Jernigan, G. G.; Jonker, B. T. Chemical vapor sensing with monolayer MoS_2. *Nano Lett.* **2013**, *13*, 668−673.

[15] Zhang, G. Z.; Wang, J. W.; Wu, Z. F.; Ouyang, W. K.; Amini, A.; Chandrashekar, B. N.; Wang, N.; Cheng, C. Shape-dependent defect structures of monolayer MoS_2 crystals grown by chemical vapor deposition. *ACS Appl. Mater. Interfaces* **2017**, *9*, 763−770.

[16] Zafar, A.; Nan, H. Y.; Zafar, Z.; Wu, Z. T.; Jiang, J.; You, Y. M.; Ni, Z. H. Probing the intrinsic optical quality of CVD grown MoS_2. *Nano Res.* **2017**, *10*, 1608–1617.

[17] Ji, Q. Q.; Zhang, Y.; Zhang, Y. F.; Liu, Z. F. Chemical vapour deposition of group-VIB metal dichalcogenide monolayers: Engineered substrates from amorphous to single crystalline. *Chem. Soc. Rev.* **2015**, *44*, 2587–2602.

[18] Li, H.; Zhang, Q.; Yap, C. C. R.; Tay, B. K.; Edwin, T. H. T.; Olivier, A.; Baillargeat, D. From bulk to monolayer MoS_2: Evolution of Raman scattering. *Adv. Funct. Mater.* **2012**, *22*, 1385–1390.

[19] Lee, C.; Yuan, H. G.; Brus, L. E.; Heinz, T. F.; Hone, J.; Ryu, S. Anomalous lattice vibrations of single and few-layer MoS_2. *ACS Nano* **2010**, *4*, 2695–2700.

[20] Jadczak, J.; Kutrowska-Girzycka, J.; Kapuściński, P.; Huang, Y. S.; Wójs, A.; Bryja, L. Probing of free and localized excitons and trions in atomically thin WSe_2, WS_2, $MoSe_2$ and MoS_2 in photoluminescence and reflectivity experiments. *Nanotechnology*, **2017**, *28*, 395702.

[21] Carozo, V.; Wang, Y. X.; Fujisawa, K.; Carvalho, B. R.; McCreary, A.; Feng, S.; Lin, Z.; Zhou, C.; Perea-López, N.; Elías, A. L. et al. Optical identification of sulfur vacancies: Bound excitons at the edges of monolayer tungsten disulfide. *Sci. Adv.* **2017, 3**, e1602813.

[22] Varshni, Y. P. Temperature dependence of the energy gap in semiconductors. *Physica* **1967**, *34*, 149–154.
[23] Wang, H. N.; Zhang, C. J.; Rana, F. Ultrafast dynamics of defect-assisted electron-hole recombination in monolayer MoS_2. *Nano Lett*. **2015**, *15*, 339–345.
[24] Sun, L. F.; Zhang, X. M.; Liu, F. C.; Shen, Y. D.; Fan, X. F.; Zheng, S. J.; Thong, J. T. L.; Liu, Z.; Yang, S. A.; Yang, H. Y. Vacuum level dependent photoluminescence in chemical vapor deposition-grown monolayer MoS_2. *Sci*. *Rep*. **2017**, *7*, 16714.
[25] Schmidt, T.; Lischka, K.; Zulehner, W. Excitation-power dependence of the near-band-edge photoluminescence of semiconductors. *Phy*. *Rev*. *B* **1992**, *45*, 8989–8994.
[26] Senthilkumar, V.; Tam, L. C.; Kim, Y. S.; Sim, Y.; Seong, M. J.; Jang, J. I. Direct vapor phase growth process and robust photoluminescence properties of large area MoS_2 layers. *Nano Res*. **2014**, *7*, 1759–1768.
[27] Ganta, D.; Sinha, S.; Haasch, R. T. 2D material molybdenum disulfide analyzed by XPS. *Surf*. *Sci*. *Spectra* **2014**, *21*, 19.
[28] Shi, H. Y.; Yan, R. S.; Bertolazzi, S.; Brivio, J.; Gao, B.; Kis, A.; Jena, D.; Xing, H. G.; Huang, L. B. Exciton dynamics in suspended monolayer and few-layer MoS_2 2D crystals. *ACS Nano* **2013**, *7*, 1072–1080.
[29] Sim, S.; Park, J.; Song, J. G.; In, C.; Lee, Y. S.; Kim, H.; Choi, H. Exciton dynamics in atomically thin MoS_2: Interexcitonic interaction and broadening kinetics. *Phy*. *Rev*. *B* **2013**, *88*, 075434.
[30] Wang, H. N.; Zhang, C. J.; Rana, F. Surface recombination limited lifetimes of photoexcited carriers in few-layer transition metal dichalcogenide MoS_2. *Nano Lett*. **2015**, *15*, 8204–8210.
[31] Wang, H. N.; Zhang, C. J.; Chan, W. M.; Manolatou, C.; Tiwari, S.; Rana, F. Radiative lifetimes of excitons and trions in monolayers of the metal dichalcogenide MoS_2. *Phy*. *Rev*. *B* **2016**, *93*, 045407.
[32] Robert, C.; Lagarde, D.; Cadiz, F.; Wang, G.; Lassagne, B.; Amand, T.; Balocchi, A.; Renucci, P.; Tongay, S.; Urbaszek, B. et al. Exciton radiative lifetime in transition metal dichalcogenide monolayers. *Phy*. *Rev*. *B* **2016**, *93*, 205423.